JMEPEG (2011) 20:522–528
DOI: 10.1007/s11665-011-9854-y

1059-9495/$19.00

Mechanical Properties of Highly Porous NiTi Alloys

Martin Bram, Manuel Köhl, Hans Peter Buchkremer, and Detlev Stöver

(Submitted June 18, 2010; in revised form October 8, 2010)

Highly porous NiTi alloys with pseudoelastic properties are attractive candidates for biomedical implants, energy absorbers, or damping elements. Recently, a new method was developed for net-shape manufacturing of such alloys combining metal injection molding with the application of suitable space-holder materials. A comprehensive study of mechanical properties was conducted on samples with a porosity of 51% and a pore size in the range of 300-500 µm. At low deformations <6%, fully pronounced pseudoelasticity was found. Even at higher strains, a shape recovery of maximum 6% took place, on which the onset of irreversible plastic deformation was superposed. Results of static compression tests were also used to calculate the energy-absorbing capacity. Fatigue of porous NiTi was investigated by cyclic loading up to 230,000 stress reversals. The failure mechanisms responsible for a reduction of shape recovery after an increased number of load cycles are discussed.

Keywords fatigue, mechanical properties, metal injection molding, porous NiTi, powder metallurgy, space-holder technique

1. Introduction

Porous NiTi alloys are promising candidates for biomedical implants due to their shape-memory properties coupled with low stiffness, good corrosion resistance, and biocompatibility (Ref 1). In the literature, several methods for producing highly porous NiTi are described. Since the 1990s, porous NiTi produced by self-propagating high-temperature synthesis (SHS) starting from elemental Ni and Ti powders has become attractive as bone substituting implant material, e.g., for spine implants (Ref 2-8). Additionally, conventional sintering (Ref 9, 10), capsule-free hot isostatic pressing (HIP) (Ref 11, 12), HIP with gas entrapment (Ref 13, 14), and spark plasma sintering (Ref 15) have been used for the production of porous NiTi, mainly for the production of samples to characterize microstructure and mechanical properties. Most of these methods lack the ability to control pore size and pore volume fraction. Especially if starting from elemental powders, the excessive formation of intermetallic phases such as Ti_2Ni, Ni_3Ti, and Ni_4Ti_3 and of TiC and $Ti_4Ni_2O_x$ leads to an embrittlement of the matrix, which may be also coupled with a loss of pseudoelastic properties. Furthermore, none of these methods allows the near-net-shape production of highly porous NiTi components without additional mechanical machining processes. To overcome these drawbacks, a new powder metallurgical method was developed for producing highly porous NiTi by combining the metal injection molding (MIM) process with the application of suitable space-holder materials (Ref 16). NaCl was found to be the preferred space-holder material, ensuring sufficient stability to withstand pressures and temperatures during the manufacturing process (Ref 17-19). If Ni-rich NiTi alloys are produced without excessive formation of secondary phases, pseudoelastic properties with shape recovery up to 8% can be expected resulting from the well-known, reversible stress-induced phase transformation (Ref 20). This behavior makes porous NiTi especially attractive for implant applications considering that human bone also reversibly recovers strains of up to 2% (Ref 21). Therefore, porous NiTi would match the mechanical properties of the human bone better than any other implant material thus reducing the risk of stress shielding to a minimum.

Aside from bone implants, pseudoelastic NiTi foams also have potential for use in energy-absorbing structures with high damping capacity. The amount of energy absorption can be well adjusted by the porosity, which can be readily changed in the range of 20-70% if the space-holder method is used for sample preparation. Possible applications could be the control of vibrations as well as the reduction of peak loads in case of shock loading (Ref 22, 23). An example of this application is seismic protection devices (Ref 24-27). The potential of porous, pseudoelastic NiTi as damping material has been little studied so far. Only a few experimental results on this topic can be found in literature (Ref 14).

In this study, NiTi samples with a porosity of 51 vol.% and pore sizes in the range of 300-500 µm were produced by metal injection molding (MIM) starting from pre-alloyed NiTi powders (50.6 at.% Ni) and NaCl particles as space-holder material. These samples were characterized regarding their mechanical properties and microstructural changes under static and dynamic conditions. To demonstrate the potential for biomedical applications, all mechanical tests were conducted at 37 °C.

2. Experimental Procedures

A pre-alloyed, spherically shaped NiTi powder with a particle size of d_{10} = 8 µm, d_{50} = 22 µm, and d_{90} = 41 µm

This article is an invited paper selected from presentations at Shape Memory and Superelastic Technologies 2010, held May 16-20, 2010, in Pacific Grove, California, and has been expanded from the original presentation.

Martin Bram, Manuel Köhl, Hans Peter Buchkremer, and **Detlev Stöver**, Forschungszentrum Jülich, Institute IEF-1, Leo-Brandt-Str, 52425 Jülich, Germany. Contact e-mail: m.bram@fz-juelich.de.

(manufactured by TLS, Bitterfeld, Germany) with a nominal Ni content of 50.6 at.% was used as starting material. Phase transformation temperatures measured by differential scanning calorimetry (DSC) were M_s = 8 °C, M_f = −21 °C, A_s = 10 °C, and A_f = 40 °C. The impurity content of the starting powder was 0.03 wt.% C and 0.04 wt.% O. For feedstock preparation, NiTi powder was mixed with a two-component binder system containing amide wax (Licowax C, Clariant, Frankfurt, Germany) and polyethylene (PE520, Clariant, Frankfurt, Germany) in a heatable kneader. The ratio of the binder components Licowax C and PE 520 was 60/40 (in vol.%). Additionally, the space-holder NaCl (d_{10} = 290 µm, d_{50} = 392 µm, d_{90} = 620 µm) was added to the feedstock. The ratio of NiTi powder/NaCl powder/binder mixture was 25/50/25 (in vol.%). The duration of the whole mixing process was 2 h. For the metal injection molding process, an Arburg 370U 700-100/100 MIM machine was used. The feedstock was heated to 145 °C and then injected into the cylindrical mold (diameter 6 mm, length 9 mm, heated to T = 45 °C) at a pressure of 100 MPa. Afterward, amide wax was removed from the samples at 150 °C in air by wicking. Then the space-holder NaCl was dissolved in a water bath at 60 °C. The space holder was completely removed after 8 h. The second binder component was decomposed by thermal treatment at 500 °C for 2 h followed by sintering the samples in vacuum ($<10^{-5}$ mbar) at 1250 °C for 10 h. All NiTi samples were characterized in the as-sintered state without additional thermal treatments. Figure 1(a) and (b) shows the surface and a cross section of the porous NiTi sample after sintering. During processing, the impurity content increased to 0.04 wt.% C and 0.14 wt.% O, which leads to the precipitation of TiC and $Ti_4Ni_2O_x$ as already known from earlier studies (Ref 28). Formation of these Ti-rich phases increases the Ni content of the matrix, which slightly decreases phase transformation temperatures. The phase transformation was also influenced by the precipitation of the metastable Ni_4Ti_3 phase during furnace cooling, which was detected by transmission electron microscopy (TEM) (not shown here). Phase transformation of the sample after sintering was characterized by DSC. In the case of martensitic transformation, superposition of weakly pronounced peaks indicates the occurrence of a multistage phase transformation, which started at 8 °C and finished completely at −120 °C. The austenitic transformation was characterized by a single peak with A_s = −8 °C and A_f = 26 °C.

In order to compare the mechanical properties, porous Ti samples were prepared in the same manner starting from a gas atomized Ti powder (manufactured by TLS, Germany) with a particle size of d_{10} = 8 µm, d_{50} = 20 µm, and d_{90} = 37 µm. The impurity content of the starting powder was 0.26 wt.% O and 0.004 wt.% C. After desalination and debinding, the samples were sintered at 1300 °C for 3 h in vacuum. Afterward, the impurity contents increased to 0.35 wt.% O and 0.04 wt.% C. The microstructure of the Ti sample is shown in Fig. 1(c).

The porosity of the samples after sintering was measured by optical analysis using analySIS® software. The amount of closed porosity was determined by the Archimedes method. The macro- and microporosity of the NiTi sample were 49.1 and 2.2%, respectively. The Archimedes method showed a total porosity of 51.4%, which is in good accordance with optical analysis. The proportion of closed pores was measured as 5.0%. For the titanium sample, the macro- and microporosity were 51.2 and 0.6%, respectively. The Archimedes method showed a total porosity of 51.3%, with a proportion of closed pores of 5.6%. The size of the macropores differs only marginally from the size of the NaCl space-holder particles (see Fig. 1). The low amount of microporosity in the case of the titanium sample clearly shows the improved sintering activity of the titanium powder when compared to the NiTi powder.

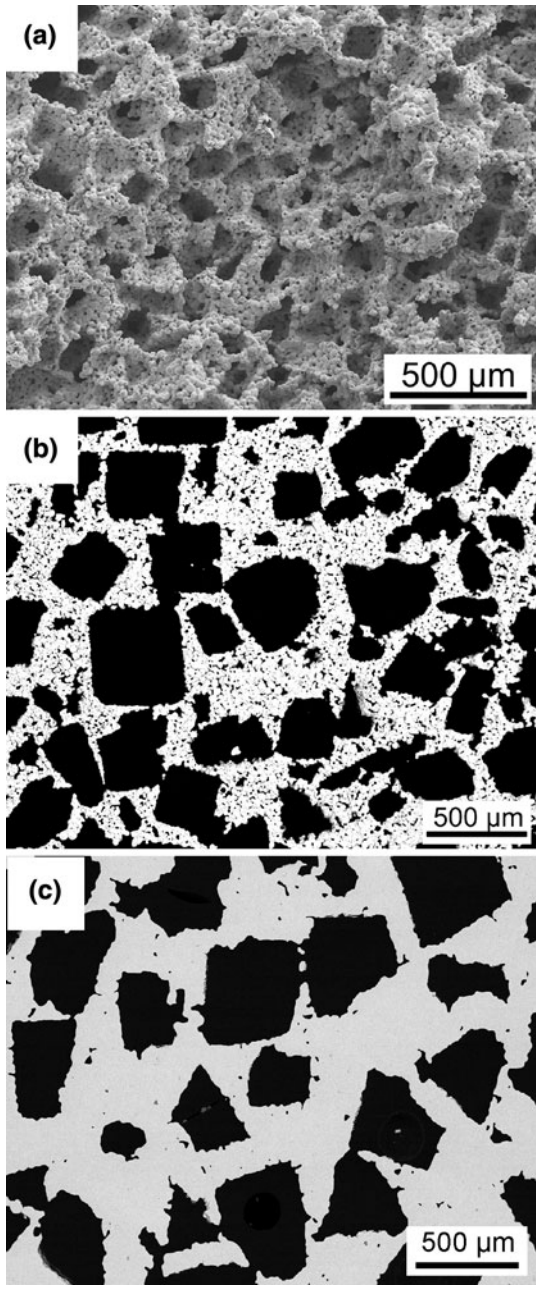

Fig. 1 Microstructure of powder metallurgical NiTi and Ti with a macroporosity of 51%. (a) NiTi, fractured surface, (b) NiTi, cross section, (c) Ti, cross section

Static compression tests were performed with an Instron-8801 testing machine at a constant temperature of 37 °C in a climate chamber. The strain was measured using an external displacement transducer. Firstly, loading-unloading cycles up to a maximum deformation of 50% were conducted on NiTi and Ti samples at a constant deformation rate of 0.5 mm/min. Then, a more detailed study to separate the amounts of pseudoelastic and plastic deformation was performed on NiTi samples

compressed to 4 and 16%. These measurements were also used to calculate the proportions of energies, which were (I) reversibly absorbed by elastic deformation ($E_{rev.}$), (II) irreversibly dissipated by stress induced, reversible phase transformation ($E_{diss.}$), or (III) irreversibly absorbed by the onset of plastic deformation ($E_{plast.}$). During each loading cycle the irreversibly absorbed energy $E_{abs.}$ is the sum of $E_{diss.}$ and $E_{plast.}$. Additionally, the fatigue of pseudoelastic properties was analyzed in more detail by strain-controlled fatigue tests. An initial loading-unloading cycle of up to 4% compression was therefore carried out at a low deformation rate of 0.5 mm/min. This cycle was then repeated up to 230,000 times at a frequency of 1 Hz (deformation rate 43 mm/min). The same test was conducted on another sample, which was pre-compressed to 16%. The microstructural change after 230,000 load cycles was investigated by metallography.

3. Results

Figure 2 compares the deformation behavior of a fully austenitic NiTi with a Ti sample, both manufactured with a porosity of 51%. The Ti sample shows the typical deformation behavior of ductile metal foams (Ref 29), where the slope of the curve during loading-unloading cycles is mainly influenced by the Young's modulus (Fig. 2b). In direct comparison, the deformation behavior of porous NiTi is characterized by a lower Young's modulus and a lower plateau stress, which was not unexpected considering the mechanical properties of the related bulk materials. Additionally, the NiTi sample shows clearly pronounced reversible shape recovery, which is still present even after high plastic deformations of up to 50% (Fig. 2a). This result is surprising since complete failure of samples was already expected at lower deformations considering the higher microporosity of sintered struts compared to porous titanium samples and the existence of brittle $Ti_4Ni_2O_x$ and TiC precipitations.

Table 1 summarizes the Young's modulus and yield strength of porous NiTi and Ti. Furthermore, Young's modulus was calculated using a model developed by Gibson and Ashby (Ref 21). In this model, the relationship between Young's modulus and relative density is given by Eq 1:

$$E^* = E_{solid.} \cdot \left(\frac{\rho^*}{\rho_{th.}}\right)^n \quad \text{(Eq 1)}$$

E^* is the Young's modulus of the porous material, $E_{solid.}$ is the Young's modulus of the bulk material, ρ^* is the relative density of the porous material, and $\rho_{th.}$ is the theoretical density of the bulk material. The model is based on a cubic, isotropic pore structure. Under this condition and if the relative density stays below 30%, it is valid that $n = 2$.

Table 1 shows that the Young's modulus can be estimated by the Gibson-Ashby equation, even if the relative density and anisotropic pore structure differ clearly from the conditions of the model. In the case of NiTi, the Young's modulus of martensite should be preferentially used for calculation.

A detailed investigation of the reversibility of shape recovery of porous NiTi samples was subsequently performed on samples compressed to 4 and 16% (Fig. 3). Figure 3(a) shows a typical loading-unloading cycle of up to 4% deformation. An almost complete shape recovery ($\varepsilon_{rev.}$) took place demonstrating fully pronounced pseudoelasticity, while the amount of irreversible plastic deformation ($\varepsilon_{irrev.}$) is almost negligible. In this study, no further differentiation was made between pseudoelastic and elastic proportions of the shape recovery ($\varepsilon_{rev.}$). At higher deformations, the onset of plastic deformation is superposed on the pseudoelasticity. In the case of a precompression of 16% (Fig. 3b), the irreversible plastic deformation ($\varepsilon_{irrev.}$) was approximately 10 %. Nevertheless,

Table 1 Young's modulus and yield strength $\sigma_{0.2}$ for NiTi and Ti with a porosity of 51%

	E (measured), GPa	$\sigma_{0.2}$ (measured), MPa	E (calculated), GPa
NiTi, 51% porosity	6.0	80	19.3 (aust.) 7.1 (mart.)
Ti, 51% porosity	22.5	140	26.0

Calculation of Young's modulus by the Gibson-Ashby Eq 1 with $n = 2$, E(Ti) = 110 GPa, ρ(Ti) = 4.50 g/cm^3 (Ref 30), E(NiTi, aust.) = 82 GPa, E(NiTi, mart.) = 30 GPa, ρ(NiTi) = 6.45 g/cm^3 (Ref 31)

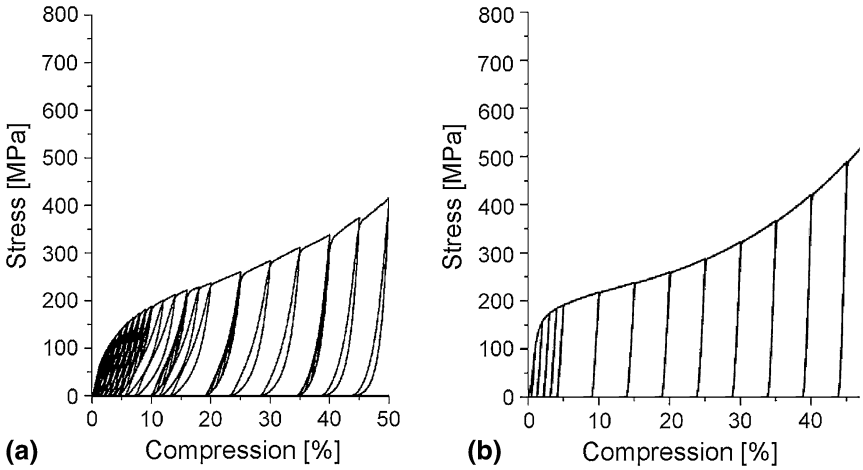

Fig. 2 Loading-unloading cycles at 37 °C with constant deformation rate of 0.5 mm/min on (a) pseudoelastic NiTi with 51% porosity and (b) Ti with 51% porosity

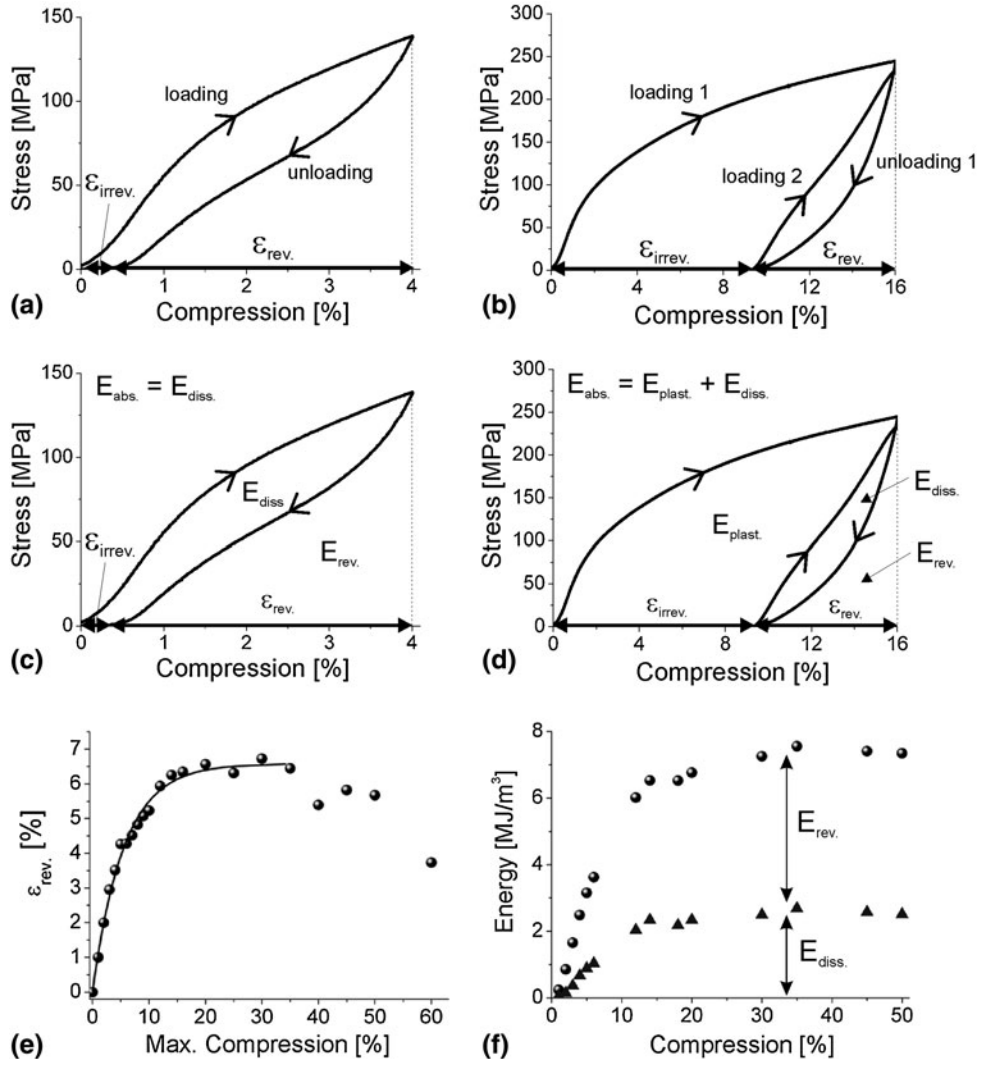

Fig. 3 Stress-compression curves on NiTi samples with 51% porosity, $T = 37$ °C. (a) fully pronounced shape recovery at 4% deformation, (b) 4% loop after a pre-compression of 16%, (c) portions of dissipated energy ($E_{diss.}$) and reversibly absorbed energy ($E_{rev.}$) in case of 4% deformation, (d) superposition of $E_{diss.}$ and $E_{rev.}$ by irreversible energy absorption due to plastic deformation ($E_{plast.}$), (e) shape recovery $\varepsilon_{rev.}$ depending on compression, and (f) proportion of reversibly absorbed energy and dissipated energy depending on compression

shape recovery ($\varepsilon_{rev.}$) of approximately 6 % still remained. Similar amounts of shape recovery were achieved for precompressions of up to 30%, after which they started to decrease again (Fig. 3e). The decrease of pseudoelasticity at higher plastic deformations is probably caused by the increased formation of microcracks homogeneously distributed all over the sintered struts in combination with an enhanced dislocation density. If a distinct level of deformation is exceeded, these microstructural changes lead to a reduced shape recovery. A detailed discussion of reasons for crack formation is given below. In Fig. 3(c) and (d), the different proportions of energy absorption are shown. At low deformations, the energy absorption is mainly related to the pseudoelastic deformation. Energy absorption is divided into a fraction of reversible absorbed energy ($E_{rev.}$), which is released again during unloading, and a fraction of dissipated energy ($E_{diss.}$), which is consumed by the reversible austenite-martensite phase transformation. No energy absorption due to plastic deformation ($E_{plast.}$) was observed in this case. With increasing deformation, the energy absorption behavior of porous NiTi approaches the behavior of conventional metal foams, which is mainly characterized by the high amount of irreversible energy absorption due to plastic deformation ($E_{plast.}$). Nevertheless, clearly pronounced amounts of energy dissipation due to phase transformations still contribute to the total absorbed energy $E_{abs.}$. Furthermore, even an energy release due to elastic shape recovery can still be found (Fig. 3f). Table 2 compares the

Table 2 Energy absorbed by irreversible plastic deformation ($E_{plast.}$)

Compression, %	NiTi (50.6 at.% Ni), 51% porosity MJ/m^3	Ti, 51% porosity MJ/m^3
6	6	9
25	47	55
50	128	156

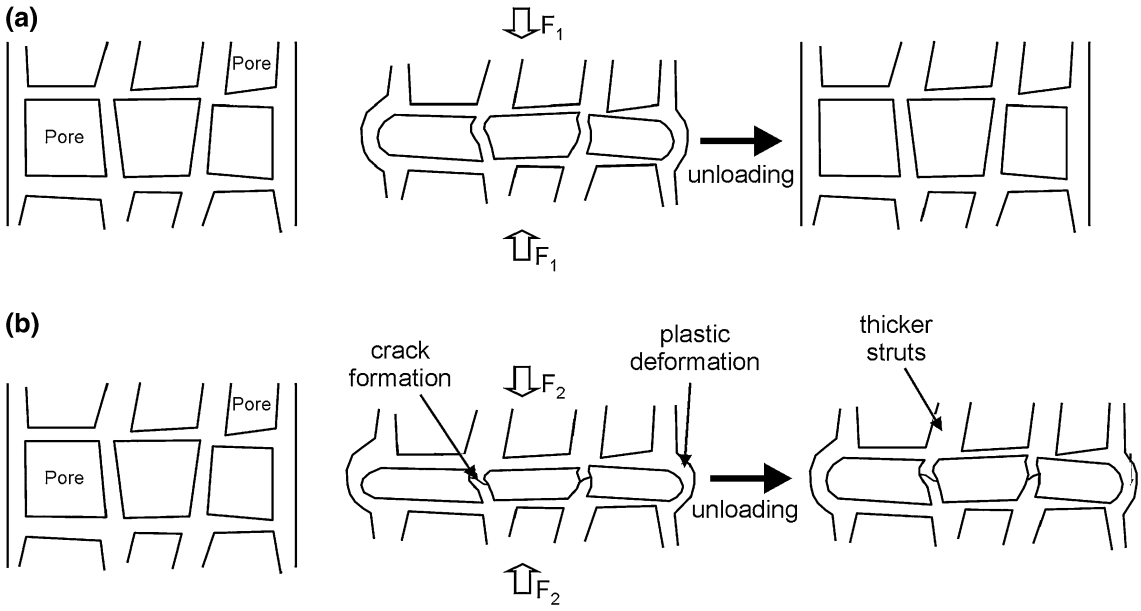

Fig. 4 Proposed deformation mechanism of pseudoelastic, porous NiTi. (a) Deformation starts at pore levels with lowest average strut thickness and (b) simultaneous plastic deformation of thin-walled levels and beginning pseudoelastic deformation of levels with enhanced wall thickness

proportions of energy irreversibly absorbed by plastic deformation ($E_{plast.}$) for pseudoelastic NiTi and Ti, both with a porosity of 51%. It becomes obvious that the energy absorption capacity of both materials lies in the same range. Slightly enhanced energy absorption of porous Ti might be explained by the reduced microporosity of the sintered struts compared to porous NiTi (Fig. 1).

As mentioned before, in the case of porous NiTi the energy absorption becomes more and more dominated by plastic deformation with increasing loads. While the ratio $E_{diss.}$:$E_{plast.}$ is approximately 1:3 at deformations of up to 10%, it changes to approximately 1:50 at deformations of 50%. Nevertheless, this small amount of residual energy dissipation could be attractive, for example, for damping of residual shock waves in the case of ballistic applications of NiTi foams.

A quite similar deformation behavior of porous NiTi samples has been reported several times in literature, even if these samples were prepared by other manufacturing routes. Li et al. (Ref 32) reported the lack of clearly pronounced stress plateau in the case of NiTi alloys with a porosity of 60-70 vol.%, which were produced by SHS (Ref 2). Furthermore, these alloys show high strain recovery, and their deformation resistance increases drastically with further strain after the elastic deformation stage. Lagoudas et al. (Ref 14) produced a porous NiTi alloy with a porosity of 42% by HIP with entrapped Ar gas. They found a gradual change in the tangent modulus beyond the elastic limit and stated that this behavior is caused by a gradual transformation of austenite into stress-induced martensite. This result was also confirmed in the work of Zhang et al. (Ref 33). A NiTi alloy with a porosity of 27 vol.% was produced by capsule-free HIP. Even at this low porosity, they did not found the typical superelasticity hysteresis loop, which is characteristic for dense NiTi alloys. An almost linear superelasticity resulted from the gradient phase transformation of pores during loading. At strain levels above 4% irreversible plastic deformation started. Nevertheless, clearly pronounced shape recovery at deformations of up to 50% was not reported in any of these publications, demonstrating the potential of our manufacturing route. Furthermore, MIM offers the possibility of net-shape manufacturing, which becomes important in the case of real applications like biomedical implants.

A mechanism to explain the specific deformation behavior of pseudoelastic NiTi foams is proposed in Fig. 4. As already known from conventional metal foams (Ref 34), deformation probably takes place level by level. Pseudoelastic deformation starts at pore levels, where the average thickness of the sintered struts (Fig. 4a) is minimal. At low deformations, pseudoelastic deformation of this level leads to an almost complete shape recovery. With increasing loads thin-walled levels start to deform plastically accompanied by crack formation, while stress-induced phase transformation occurs simultaneously at levels with enhanced average thickness of the struts (Fig. 4b). This model is in accordance with the publication of Lagoudas et al. (Ref 14), who explained that the failure of porous NiTi alloys started locally followed by a failure of neighboring regions.

In Fig. 5, first results of the fatigue of pseudoelasticity are shown. If the porous NiTi samples were cyclically loaded up to 4% (Fig. 5a), shape recovery was already reduced to 3% after 1,000 cycles. If the test was continued up to 230,000 cycles, a residual shape recovery of approximately 1% remained. If the samples were precompressed to 16% before starting loading-unloading cycles, a complete failure of the sample was already found after 900 cycles (Fig. 5b).

A similar fatigue test was conducted recently by Guo et al. on a NiTi alloy with a porosity of 64 vol.%, which was produced by SHS (Ref 35). In this study, compression loads of up to 120 MPa were repeated up to 200 times at a frequency of 1 Hz. A serrated stress-strain curve was observed in the first cycle, which was explained by the generation and propagation of microcracks. With increasing number of load cycles, the stress-strain curve becomes stable and the amount of irreversible plastic deformation introduced by each cycle decreased. A direct comparison to our results becomes difficult because Guo et al. conducted their fatigue tests at a temperature, where the

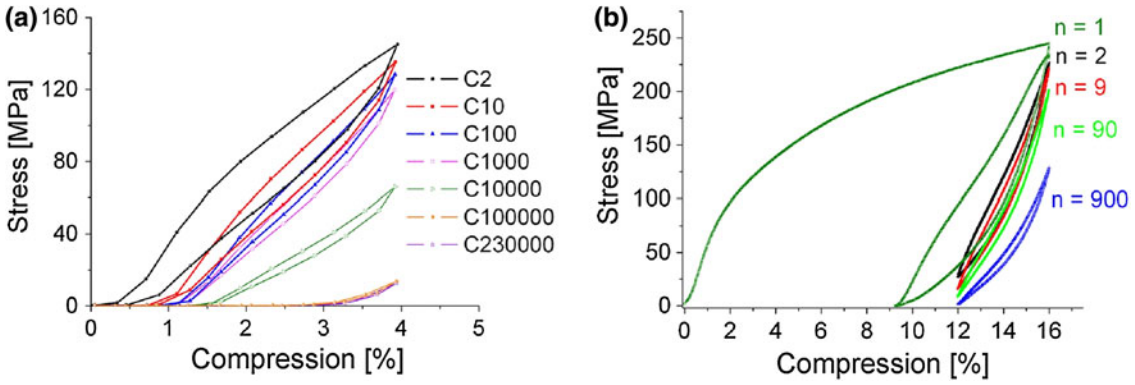

Fig. 5 (a) Fatigue of pseudoelastic properties of porous NiTi at cyclic loading up to 4% compression and (b) same measurement after a pre-compression of 16%

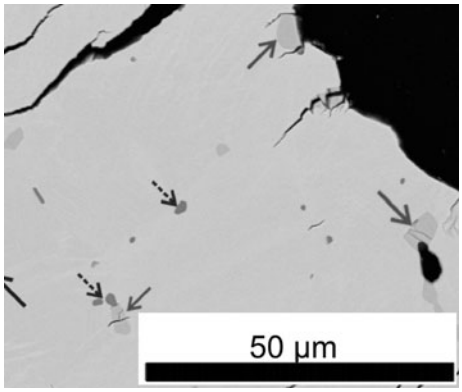

Fig. 6 Failure analysis by SEM after 230,000 load cycles. Cracks were initiated mainly from $Ti_4Ni_2O_x$ phases and micropores

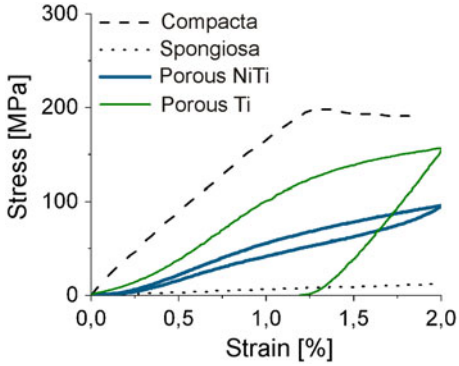

Fig. 7 Comparison of deformation behavior of porous NiTi, porous Ti (both with 51% porosity) and human bone (Ref 21). Fully pronounced pseudoelasticity of porous NiTi would reduce the risk of stress-shielding in case of implant application

sample was not fully austenitic. In other publications, functional fatigue of porous NiTi alloys has been investigated only at moderate conditions. For example, Zhang et al. (Ref 33) repeated load cycles four times, where the maximum strain was varied between 4 and 8%. They found a degradation of superelasticity only in the first cycle (almost independent from the strain), thereafter a good linear superelasticity was maintained in all cases.

In this study, the parameters of the fatigue tests were quite harsh, but they help to understand the failure mechanisms of highly porous NiTi produced by our method. Figure 6 shows the microstructure of a sintered strut after conducting 230,000 load cycles up to 4% deformation. It is obvious that the failure of the sample is mainly caused by the formation of microcracks. As already reported in earlier studies, these microcracks were preferentially initiated by brittle $Ti_4Ni_2O_x$ phases as well as by micropores and surface roughness of the sintered struts (Ref 28). If the samples are prepared by metal injection molding, further reduction of the impurity phases seems to be difficult considering the high amount of organic binders required for the MIM process. Therefore, reduction of microporosity, for example, by sintering with partial liquid phase seems to be a more promising alternative (Ref 36).

Even if the application of porous NiTi as an implant material is still a matter of controversy due to the high content of toxic Ni (Ref 37), the mechanical properties of this material recommend it as a bone-substituting material. In Fig. 7, the stress-compression curve of porous NiTi is compared with the deformation behavior of porous titanium as well as of the two main structures of human bone—compacta and spongiosa. It has been found that in the case of pseudoelastic NiTi with 51% porosity, the properties of porous NiTi match the properties of the spongious bone quite well (Ref 21), which would clearly reduce the risk of stress shielding.

4. Conclusions

Net-shaped NiTi parts with 51% porosity were produced by a combination of metal injection molding MIM with a suitable space-holder material (NaCl). Fully pronounced pseudoelastic properties were measured up to deformations of 6% demonstrating the potential, for example, for biomedical bone implants. Based on the results, it is postulated that porous NiTi matches the mechanical properties of the human bone better than any other metallic implant material thus reducing the risk of stress shielding to a minimum. In the case of higher deformations, the onset of irreversible plastic deformation was superposed more and more on the pseudoelasticity. Nevertheless, even after compression of up to 50%, a clearly pronounced amount of pseudoelastic shape recovery was found, which was not expected to this extent. In order to explain this behavior, a

deformation mechanism is proposed, which is based on a level-by-level deformation depending on the varying wall thickness of the sintered struts. For an investigation of the fatigue of pseudoelasticity, an increased number of loading-unloading cycles were conducted at high deformation rates (43 mm/min). Even after 230,000 cycles of up to 4%, a residual shape recovery of 1% was found. The main reason for the loss of functionality is the formation of microcracks in the sintered struts, which was initiated by brittle $Ti_4Ni_2O_x$ phases, micropores, and the residual surface roughness of the sintered struts.

Acknowledgments

The authors thank the Deutsche Forschungsgemeinschaft DFG for financially supporting this work (SFB459: Shape Memory Technology). The support of Prof. Dr. Tilman Beck and Mr. Alexander Moser for mechanical characterizations as well as Mr. Mark Kappertz and Dr. Doris Sebold for metallographical investigations is gratefully acknowledged.

References

1. A. Bansiddhi, T.D. Sargeant, S.I. Stupp, and D.C. Dunand, Porous NiTi for Bone Implants: A Review, *Acta Biomater.*, 2008, **4**, p 773–782
2. V.I. Itin, V.E. Gjunter, S.A. Shabaloyskaya, and R.L.C. Sacheva, Mechanical Properties and Shape Memory of Porous Nitinol, *Mater. Character.*, 1994, **32**, p 179–187
3. A. Biswas, Porous NiTi by Thermal Explosion Mode of SHS: Processing, Mechanism and Generation of Single Phase Microstructure, *Acta Mater.*, 2005, **53**, p 1415–1425
4. C.L. Chu, C.Y. Chung, P.H. Lin, and S.D. Wang, Fabrication of Porous NiTi Shape Memory Alloy for Hard Tissue Implants by Combustion Synthesis, *Mater. Sci. Eng. A*, 2004, **366**, p 114–119
5. C.L. Chu, Fabrication and Properties of Porous NiTi Shape Memory Alloys for Heavy Load-Bearing Medical Applications, *J. Mater. Process. Technol.*, 2005, **169**, p 103–107
6. B.Y. Li, L.J. Rong, Y.Y. Li, and V.E. Gjunter, Synthesis of Porous Ni-Ti Shape-Memory Alloys by Self-Propagating High-Temperature Synthesis: Reaction Mechanism and Anisotropy in Pore Structure, *Acta Mater.*, 2000, **48**, p 3895–3904
7. C.L. Yeh and W.Y. Sung, Synthesis of NiTi Intermetallics by Self-Propagating Combustion, *J. Alloys Compd.*, 2004, **376**, p 79–88
8. M. Assad, F. Likibi, P. Jarzem, M.A. Leroux, C. Coillard, and C.H. Rivard, Porous Nitionol vs. Titanium Intervertebral Fusion Implants: Computer Tomography, Radiological and Histological Study of Osseointegration Capacity, *Mat. Werkst.*, 2004, **35**, p 219–223
9. B.Y. Li and L.J. Rong, Porous NiTi Alloy Prepared from Elemental Powder Sintering, *J. Mater. Res.*, 1997, **13**, p 2847–2851
10. S.L. Zhu, X.J. Yang, D.H. Fu, L.Y. Zhang, C.Y. Li, and Z.D. Cui, Stress-Strain Behavior of Porous NiTi Alloys Prepared by Powders Sintering, *Mater. Sci. Eng. A*, 2005, **408**, p 264–268
11. S. Wu, C.Y. Chung, X. Liu, P.K. Chu, J.P.Y. Ho, C.L. Chu, Y.L. Chan, K.W.K. Yeung, W.W. Lu, K.M.C. Cheung, and K.D.K. Luk, Pore Formation Mechanism and Characterization of Porous NiTi Shape Memory Alloys Synthesized By Capsule-Free Hot Isostatic Pressing, *Acta Mater.*, 2007, **55**, p 3437–3451
12. B. Yuan, X.P. Zhang, C.Y. Chung, and M. Zhu, The Effect of Porosity on Phase Transformation Behavior of Porous Ti–50.8 at.% Ni Shape Memory Alloys Prepared by Capsule-Free Hot Isostatic Pressing, *Mater. Sci. Eng. A*, 2006, **438**, p 585–588
13. C. Greiner, S.M. Oppenheimer, and D.C. Dunand, High Strength, Low Stiffness, Porous NiTi with Superelastic Properties, *Acta Biomater.*, 2005, **1**, p 705–716
14. D.C. Lagoudas and E.L. Vandygriff, Processing and Characterization of NiTi Porous SMA by Elevated Pressure Sintering, *J. Intell. Mater. Syst. Struct.*, 2002, **13**, p 837–850
15. Y. Zhao, M. Taya, Y. Kang, and A. Kawasaki, Compression Behavior of Porous NiTi Shape Memory Alloy, *Acta Mater.*, 2005, **53**, p 337–343
16. M. Köhl, T. Habijan, M. Bram, H.P. Buchkremer, D. Stöver, and M. Köller, Powder Metallurgical Near-Net-Shape Fabrication of Porous NiTi Shape Memory Alloys for Use as Long-Term Implants by the Combination of the Metal Injection Molding Process with the Space-Holder Technique, *Adv. Eng. Mater.*, 2009, **11**, p 959–968
17. M. Köhl, J. Mentz, M. Bram, H.P. Buchkremer, and D. Stöver, Production of Highly Porous Near-Net-Shape NiTi Components for Biomedical Applications, *Conference on Porous Metals and Metallic Foams METFOAM 2007*, DEStech. Publication, 2008, p 295–298
18. A. Bansiddhi and D.C. Dunand, Shape-Memory NiTi Foams Produced by Solid-State Replication with NaF, *Intermetallics*, 2007, **15**, p 1612–1622
19. A. Bansiddhi and D.C. Dunand, Shape-Memory NiTi Foams Produced by Replication of NaCl Space-Holders, *Acta Biomater.*, 2008, **4**, p 1996–2007
20. K. Otsuka and C.M. Waymann, *Shape Memory Materials*, Cambridge University Press, Cambridge, 1998
21. L.J. Gibson and M.F. Ashby, *Cellular Solids*, Cambridge University Press, Cambridge, 1997
22. W. Predki, M. Klönne, and A. Knopik, Cyclic Torsional Loading of Pseudoelastic NiTi Shape Memory Alloys: Damping and Fatigue Failure, *Mater. Sci. Eng. A*, 2006, **417**, p 182–189
23. E. Pieczyska, S. Gadaj, W.K. Nowacki, K. Hoshio, and Y. Makino, Characteristics of Energy Storage and Dissipation in TiNi Shape Memory Alloy, *Sci. Technol. Adv. Mater.*, 2005, **6**, p 889–894
24. R. Fosdick and Y. Ketema, Shape Memory Alloys for Passive Vibration Damping, *J. Intell. Mater. Syst. Struct.*, 1998, **9**, p 854–870
25. P. Thomson, G.J. Balas, and P.H. Leo, The Use of Shape Memory Alloys for Passive Structural Damping, *Smart Mater. Struct.*, 1995, **4**, p 36–41
26. M. Dolce and D. Cardone, Mechanical Behaviour of Shape Memory Alloys for Seismic Applications 1. Martensite and Austenite NiTi Bars Subjected to Torsion, *Int. J. Mech. Sci.*, 2001, **43**, p 2632–2656
27. M. Dolce and D. Cardone, Mechanical Behaviour of Shape Memory Alloys for Seismic Applications 2. Austenite NiTi Wires Subjected to Tension, *Int. J. Mech. Sci.*, 2001, **43**, p 2657–2677
28. J. Mentz, M. Bram, H.P. Buchkremer, and D. Stöver, Improvement of Mechanical Properties of Powder Metallurgical NiTi Shape Memory Alloys, *Adv. Eng. Mater.*, 2006, **8**, p 247–252
29. T. Imwinkelried, Mechanical Properties of Open-Pore Titanium Foam, *J. Biomed. Mater. Res. A*, 2007, **81**, p 964–970
30. M. Peters and C. Leyens, *Titan und Titanlegierungen*, Wiley-VCH, Weinheim, 2002
31. http://www.memry.com/resources/faq-properties.php, released 2010
32. B.Y. Li, L.J. Rong, Y.Y. Li, and V.E. Gjunter, An Investigation of the Synthesis of Ti-50 at. pct Ni Alloys Through Combustion Synthesis and Conventional Powder Sintering, *Metall. Mater. Trans.*, 2000, **A31**, p 1867–1871
33. X.P. Zhang, H.Y. Liu, B. Yuan, and Y.P. Zhang, Superelasticity Decay of Porous NiTi Shape Memory Alloys Under Cyclic Strain-Controlled Fatigue Conditions, *Mater. Sci. Eng.*, 2008, **A481–482**, p 170–173
34. J. Banhart, Manufacture, Characterisation and Application of Cellular Metals and Metal Foams, *Prog. Mater. Sci.*, 2001, **46**, p 559–632
35. Z. Guo, H. Xie, F. Dai, H. Qiang, L. Rong, P. Chen, and F. Huang, Compressive Behavior of 64% Porosity NiTi Alloy: An Experimental Study, *Mater. Sci. Eng.*, 2009, **A515**, p 117–130
36. A. Bansiddhi and D.C. Dunand, Shape-Memory NiTi-Nb Foams, *J. Mater. Res.*, 2010, **24**, p 2107–2117
37. S.A. Shabalovskaya, Surface, Corrosion and Biocompatibility Aspects of Nitinol as an Implant Material, *Biomed. Mater. Eng.*, 2002, **12**, p 69–109